Analysis of Compensation Ratios and Control Torques of an Axial Piston Pump with Rotated Valve Plates

Thomas Heeger[1], Stephan Wegner, Liselott Ericson[1]

[1]*The Division of Fluid and Mechatronic Systems, The Department of Management and Engineering, Linköping University,* thomas.heeger@liu.se

Abstract

Conventionally, variable hydraulic axial piston machines vary displacement by adjusting the length of the piston stroke. Another method to achieve variable displacement is to rotate the valve plate and thus adjust the effective use of the piston stroke. This paper provides an analytical methodology to calculate control torques for valve plate rotation. This methodology considers compensation ratios in the contact between the valve plate and the piston plate, and compensation ratios in the contact between the valve plate in the housing. This paper adds the consideration of a spring force, pressure-dependent viscosity, and a surrogate model for the compensation force from the area between high-pressure and low-pressure to the traditional calculation of the compensation ratio. The influence of the cylinder barrel's rotation angle and the valve plate rotation angle is taken into account. The calculation results for an exemplary pump of floating piston type reveal that the main share of the required control torque originates from the contact between the valve plate and the housing. A hydrostatic compensation force in that interface can reduce this torque, but it is illustrated that a full compensation is not possible. For large valve plate rotation angles, the risk of valve plate tipping caused by the axial ports in the housing is shown, which shows that valve plate rotation is not suitable for displacement control to small displacement levels when using axial ports.

River Journal, 1–27.

Keywords: axial piston pump, variable displacement, valve plate rotation, compensation ratio, control torque, double pump.

1 Introduction

Variable displacement in hydraulic machines can avoid the delivery of hydraulic excess power and enable the downsizing of the prime mover. Typically, the displacement is varied by adjusting the length of the piston stroke, e.g., by adjusting the angle of the swash plate in swash plate machines. Another possibility to achieve variable displacement is to rotate the valve plate (VP) and thus adjust the effective use of the piston stroke.
Expected benefits of VP rotation are small control torques and low actuation power, and thus an easy control [1]. The power required for the displacement control can have a significant share of the system losses, as the overall efficiency of displacement controlled pumps can be significantly reduced by their control power [12].
The idea of VP rotation is not new, and the concept has already been studied decades ago. Small VP rotations, by only a couple of degrees, have been considered in order to adjust the effective pre-compression in a pump (e.g. [4,8]), while large VP rotations have been considered in order to vary pump displacement by reducing the effective piston stroke [7, 15]. Unfortunately, the same pre and de-compression angles provide a higher effective pre and de-compression when commutation takes place at a greater distance to the dead centres. When pre and de-compression angles cannot be modified for different operating points and displacement settings, issues such as cavitation and high-pressure (HP) peaks [3] as well as noise and backflow [5] occur. Using a double pump with opposing pistons as sketched in Fig. 1 offers the potential to overcome these obstacles: as visualised in Fig. 2, the displacement can be adjusted by joint rotation of both VPs, and the effective pre and de-compression can be adjusted by relative rotation of the VPs. [9]

When rotating a VP, all of its tasks need to be considered: VPs are used to separate the inlet from the outlet as well as to provide a smooth pressure transition for each piston chamber as it passes over the valvelands between inlet and outlet. Furthermore, they provide an axial journal to balance the piston forces, which needs to provide a good compromise between frictional and leakage losses. Conventionally, on the backside of the VP, no relative movement to the housing takes place, and thus the focus is solely on avoiding leakage losses, which means that a compensation of the piston forces is not desired in that interface. [13] When rotating the VP, of course, this needs to

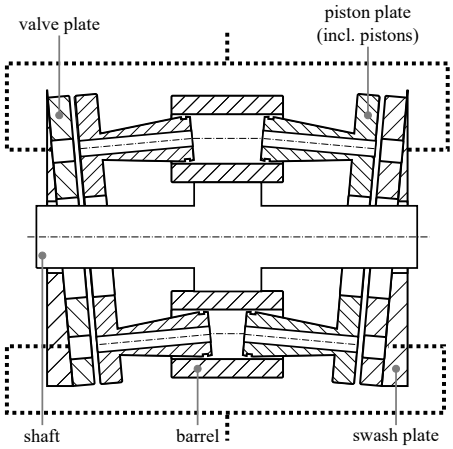

Figure 1: Floating piston pump with opposing pistons. Two opposing pistons share one bore in the cylinder barrel, and therefore they communicate with one another.

be revisited. A (partial) compensation of the piston forces is then desired in order to reduce the torque required to move the VP.
The required control torque is dependent on the cylinder barrel (CB) rotation angle and the VP rotation angle. This paper presents an analytical methodol-

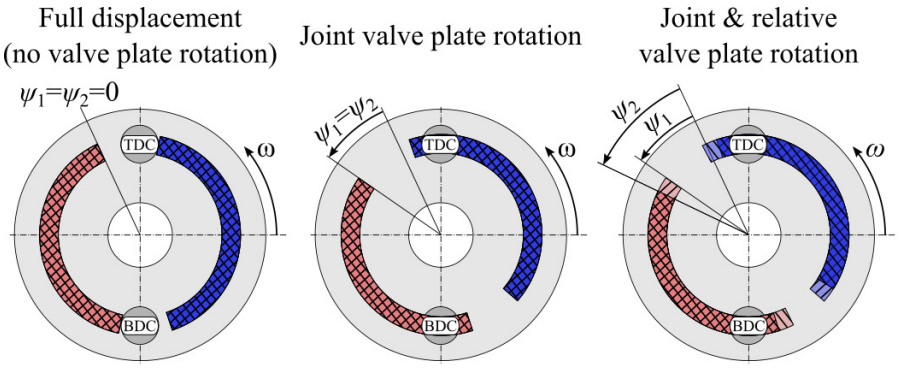

Figure 2: Joint and relative VP rotation. Left: both VPs are in the same position (at maximum displacement). Center: both VPs have been rotated by the same angle, reducing the displacement. Right: VP2 has been rotated by an additional angle, reducing the pre- and de-compression angle.

ogy to calculate compensation ratios and quantify the required control torque for different CB and VP rotation angles. This is done on the example of a floating piston pump [6] with opposing pistons. For this purpose, the consideration of a spring force, pressure-dependent viscosity and a surrogate model for the compensation force from the area between HP and low-pressure (LP) are added to the traditional calculation of the compensation ratio. Furthermore, the balance point (BP) of the uncompensated force is calculated to evaluate the risk of VP tipping and a VP modification for decreased control torques is suggested.

2 Methodology

Forces in axial piston machines can be distinguished between pressure-dependent and pressure-independent forces. Pressure-dependent forces occur due to the pressurisation of an area and are the dominant type of force in hydrostatic machines. Even frictional forces are dominantly pressure-dependent. Typically, it is attempted to compensate pressure-dependent forces in contacts with relative motion by hydrostatic bearings. [10]

2.1 Analysis of Compensation Ratios

Traditionally, the compensation ratio ζ is defined as the ratio between loading forces and compensating fluid forces in the important contact between VP and cylinder block, see (1). The equivalent contact in the machine sketched in Fig. 1 is the contact between VP and piston plate (PP). The VPs are parallel to the swash plates, and the piston forces act normal to the VPs. Therefore, compensation ratios for the pump sketched in Fig. 1 and for traditional swash plate pumps can be calculated with the same methodology.

$$\zeta = \frac{F_{\mathrm{comp}}}{F_{\mathrm{load}}} \tag{1}$$

A compensation ratio larger than 1 indicates that the cylinder block resp. PP can lose contact to the VP, leading to uncontrolled leakage of HP fluid which can cause a loss of functionality. Compensation ratios far below 1 indicate solid body contact, which leads to the risk of wear and fretting. [4] Therefore, compensation ratios slightly below 1 are targeted in the design process (see [10, 17]).
As the calculation methods for ζ in the literature differ, the correct interpretation of the numerical value of the compensation ratio depends on the used

method. Wegner et al. [17] summarises and compares different methods for analytical calculation of the compensation ratio of the contact between VP and cylinder block.

2.1.1 Assumptions and Simplifications

As summarised in [18], numerical models can take into account non-uniform gap heights, elastic and thermal deformation as well as hydrodynamic and squeezing effects. However, when attempting to calculate compensation ratios analytically, some assumptions and simplifications are typically made (see [13, 17]):

- All pressurised pistons are at the same pressure level.
- The contact surfaces are flat and parallel to one another. The gap height is constant over time and there is no tipping of the cylinder block resp. PP. Therefore, no squeeze flows are present.
- There is no relative motion between the contact surfaces. Therefore, no shear flows are present.
- The fluid has a constant density (i.e., it is incompressible) and a constant viscosity. This simplifies the expression for the pressure flow. However, in this paper, pressure-dependency of the viscosity is considered using (7).
- Only forces generated by static pressure are considered. Other forces (e.g., hydrodynamic forces) are neglected. However, in this paper, the spring force pressing the PP against the VP is also considered.

Some of the assumptions are further elaborated and justified in [4]. In this paper, effects such as elastic and thermal deformation, and production influences are not considered.
The PP is floating and its position is affected by the contact points between PP and CB. However, this is neglected in this paper. Instead it is assumed that the centre of gravity of the PP remains at the same location, i.e., the PP only moves around its axis and does no translational movement relative to the VP.

2.1.2 Load Force

Fig. 3 sketches the piston force and the compensation force for the contact PP-VP. The load force for this contact is created by the pressurised pistons. Wegner et al. [17] emphasizes that some methods consider the passage opening area as loaded area, i.e., a pressure force from this area is used both for the calculation of F_{comp} and F_{load}. However, in the passage opening of a kidney, no load on the PP-VP contact is created. Therefore, there is no physical

equivalent to this calculated pressure force, and compensation ratios would be overestimated. [17] Thus, (2) considers that no load on the PP is created at the passage areas A_{pass} through the piston bores. Furthermore, the spring force F_{S} pressing the PP against the VP is considered.

$$F_{\mathrm{load,PP-VP}} = \sum_i p_i \left(A_{\mathrm{piston}} - A_{\mathrm{pass}}\right) + F_{\mathrm{S}} \tag{2}$$

The same methodology can be applied to calculate the load force in the

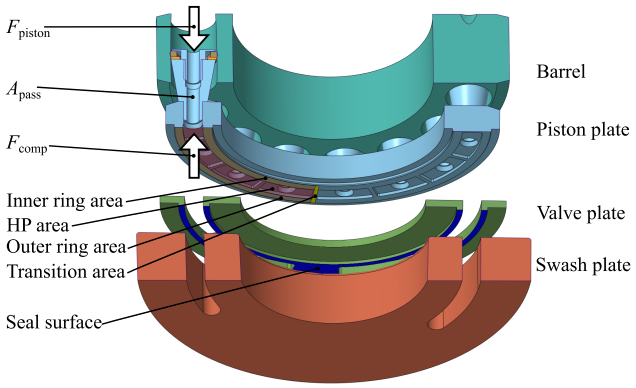

Figure 3: Overview of relevant pump parts and pressure zones for the contact PP-VP.

contact between the VP and the housing (contact VP-H), which is sketched in Fig. 4. The pressurised area in the HP kidney does not lead to a force in this contact, as that pressure force is taken by the housing. Hence the load force is calculated acc. to (3).

$$F_{\mathrm{load,VP-H}} = \left(\sum_i p_i A_{\mathrm{piston}}\right) - p_H A_{\mathrm{kidney}} + F_{\mathrm{S}} \tag{3}$$

2.1.3 Compensation Force

To calculate the compensation force, the pressure distribution in the different contact areas needs to be known. Thus different areas are defined, in which the pressure distribution can be described. For the contact PP-VP, these areas are marked in Fig. 3 and 5. The compensation force is calculated in (4):

$$F_{\mathrm{comp}} = F_{\mathrm{HP}} + F_{\mathrm{rings}} + F_{\mathrm{trans}} \tag{4}$$

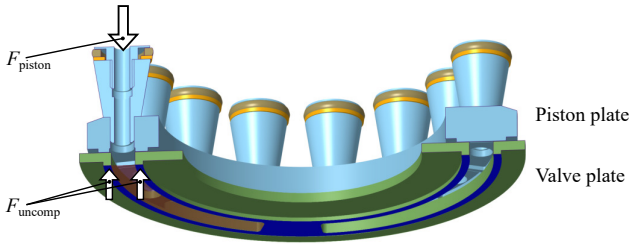

Figure 4: The contact VP-H is typically not compensated and acts as a seal. The load force is created by the pistons, and the kidney opening reduces the force in the contact.

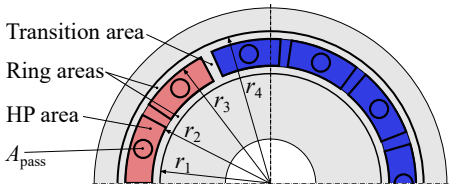

Figure 5: Relevant areas in contact PP-VP and definition of r_1 to r_4.

For calculation of F_{HP} in the contact PP-VP, HP is present in the areas covered by a pocket connected to the HP kidney. At the passage areas A_{pass} no compensation force is created.

$$F_{\text{HP,PP-VP}} = p_{\text{H}} \left(r_3^2 - r_2^2\right) \left(\varphi_{\text{E}} - \varphi_{\text{S}}\right)/2 - \sum_i p_i A_{\text{pass}} \tag{5}$$

In the contact VP-H, conventionally no compensation force is desired. The high piston forces are actually appreciated as they guarantee a good sealing in this contact, which avoids leakage losses. Typically, the backside of the VP provides no area for HP to act upon. However, this changes for increased VP rotation angles, see sec. 2.2.3.
Besides the calculation of F_{HP}, the forces at the ring areas F_{rings} and the transition areas between the HP and LP zones F_{trans} need to be calculated. When calculating these forces for the contact VP-H, two different assumptions can be made:

1. The load force strongly dominates over the compensation force, thus the contact is perfectly sealed and no hydrostatic force is present, i.e.,

$F_{\mathrm{rings,VP-H}} = 0$ and $F_{\mathrm{trans,VP-H}} = 0$. This assumption applies for very low compensation ratios.

2. There is leakage between the housing and the VP, which enables communication of pressure. The pressure distribution is similar to the one in the contact between PP and VP. This assumption applies for higher compensation ratios.

For the calculation of F_{rings} for the contact VP-PP, or contact VP-H with assumption 2, the Reynolds equation (6) can be simplified and an analytical solution is possible. Equation (6) consists of terms for squeeze flow, shear flow and pressure flow [17].

$$\frac{\partial\left(\rho h\right)}{\partial t} + \nabla \cdot \left(\frac{\rho h}{2}\left(\vec{v_{\mathrm{t}}} + \vec{v_{\mathrm{b}}}\right)\right) - \nabla \cdot \left(\frac{\rho h^3}{12\eta}\nabla p\right) = 0 \tag{6}$$

With the assumptions given in sec. 2.1.1 and the pressure-dependent viscosity as in (7) [14], only the term for pressure flow remains and is simplified to (8).

$$\eta = \eta_0\, e^{bp} \tag{7}$$

$$\nabla \cdot e^{-bp}\,\nabla p = 0 \tag{8}$$

Equation (8) written in cylinder coordinates, and a constant pressure over φ and z, yield in (9).

$$\frac{\partial^2 p}{\partial r^2} - b\left(\frac{\partial p}{\partial r}\right)^2 = 0 \tag{9}$$

Integrating twice, and the boundary values ($p(R_{\mathrm{O}}) = p_{\mathrm{O}}$, $p(R_{\mathrm{I}}) = p_{\mathrm{I}}$), yield in (10).

$$p\left(r\right) = p_{\mathrm{O}} - \frac{1}{b}\ln\left(\frac{(R_{\mathrm{O}} - r)e^{b(p_{\mathrm{O}} - p_{\mathrm{I}})} + r - R_{\mathrm{I}}}{R_{\mathrm{O}} - R_{\mathrm{I}}}\right) \tag{10}$$

An example for the resulting pressure distribution is shown in Fig. 6.

The pressure force and its BP can generally be calculated using (11) and (12), and if desired the BP be converted to polar coordinates using (13).

$$F = \int_{\varphi_{\mathrm{S}}}^{\varphi_{\mathrm{E}}} \int_{R_{\mathrm{I}}}^{R_{\mathrm{O}}} p(r)\, r\, dr\, d\varphi \tag{11}$$

$$x_{\mathrm{bp}} = \left(\int_{\varphi_{\mathrm{S}}}^{\varphi_{\mathrm{E}}} \int_{R_{\mathrm{I}}}^{R_{\mathrm{O}}} p(r) r^2 \cos\varphi\, dr\, d\varphi\right)/F \tag{12a}$$

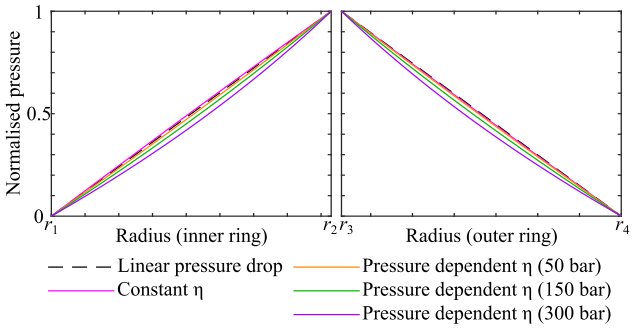

Figure 6: Normalised pressure distribution over ring areas.

$$y_{\mathrm{bp}} = \left(\int_{\varphi_{\mathrm{S}}}^{\varphi_{\mathrm{E}}} \int_{R_{\mathrm{I}}}^{R_{\mathrm{O}}} p(r) r^2 \sin\varphi \, dr \, d\varphi \right) / F \tag{12b}$$

$$r_{\mathrm{bp}} = \sqrt{x_{\mathrm{bp}}^2 + y_{\mathrm{bp}}^2} \tag{13a}$$

$$\varphi_{\mathrm{bp}} = \mathrm{arctan2}(x_{\mathrm{bp}}, y_{\mathrm{bp}}) \tag{13b}$$

The estimation of the pressure field in the transition zones underlies a high degree of uncertainty. Thus it is often not considered for the calculation of the compensation ratio, or different assumptions are made to calculate the pressure force. [17]
In this paper, the pressure distribution in the contact VP-H is calculated using the EHD simulation program described in [16], utilizing the basic functionality of modelling the geometry and solving the Reynolds equation using the finite volume method discretised model. It allows to add features like kidneys and bores as boundary conditions to a disc-shaped simulation domain. In this work, it is used as a tool to calculate the pressure distribution in the transition zones where analytical calculations cannot be applied. The simulation results are condensed in a surrogate model in order to enable analytical calculations. More details are presented in sec. 2.2.3.

2.2 Cylinder Barrel Rotation and Valve Plate Rotation Dependent Compensation Ratios

Typically, the compensation ratio is only calculated for one rotational position of the CB. However, the compensation ratio varies over the cylinder block rotation angle [11] resp. the CB rotation angle, and also over the VP rotation angle.

2.2.1 Load Force

Firstly, the load force needs to be calculated. Hence, the pressure in each chamber needs to be known. Lee et al. [11] assumes the piston chamber pressures to remain at the pressure of the last kidney the chamber was in contact with, i.e., the chamber reaches HP when entering the HP kidney and remains at this pressure level until entering the LP kidney. This approach can also be applied for rotated VPs.

Figure 7a shows the start and end of the HP kidney (α_S, α_E) and the LP kidney (β_S, β_E). The kidney angles need to reflect the current kidney angles under consideration of the VP rotation. As the two sides of the pump communicate with one another through the CB, relative valve plate rotation needs to be considered. For the contact PP-VP, the effective VP angles are to be used, see Fig. 2.

At commutation from LP to HP, a chamber reaches HP as soon as it gets in contact with a HP kidney at α_S. The pocket in the PP then extends the HP area by the angle θ_3, and over the angle θ_4 the pressure drops to LP level. At commutation from HP to LP, the chamber pressure drops to LP as soon as the chamber gets in contact with a LP kidney at β_S. Thus the HP area reaches at least to the angle $\beta_{\mathrm{S}'} = \beta_\mathrm{S} - 2\pi/z$, which is one period before the start of the LP kidney at β_S. The HP area on the interface VP-PP is extended beyond $\beta_{\mathrm{S}'}$ by the angle θ_1, and over the angle θ_2 the pressure drops to LP level.

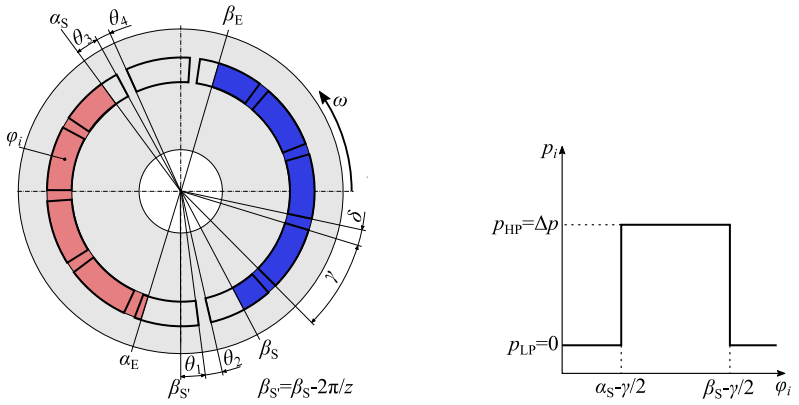

(a) Definition of relevant angles around commutation. The HP kidney is marked in red, the LP kidney is marked in blue.

(b) Pressure p_i in one chamber i over rotational angle of the chamber φ_i.

Figure 7: View of VP and port plate angles as well as chamber pressure.

2.2.2 Compensation Force in Contact between Piston Plate and Valve Plate

Lee et al. [11] introduces case differentiations for different situations around commutation. In this paper, a lower number of cases is required as both the pockets in the PP and the kidneys are rectangular. For each commutation, four different situations are possible as shown in Fig. 8 and 9. For each of the cases, two angles can be calculated: the angle extending the length of the HP area (θ_1, θ_3), and the angle of the transition area between HP and LP (θ_2, θ_4). These angles are used to provide inputs to (5), (11) and (16) for different CB and VP rotation angles. The equations for the calculation of the angles are shown in tab. 1. For the calculation of F_{trans}, case 1 of the surrogate model developed for the contact VP-H is used, see sec. 2.2.3.
Furthermore, cross-porting can be considered. When cross-porting occurs, it is assumed that the kidneys keep their pressure levels, and that in the chamber connecting HP and LP, the pressure is $(p_{\mathrm{H}} + p_{\mathrm{L}})/2$. Cross-porting can occur for large relative VP rotation angles, and small cross-porting angles might be desired in some operating points in order to reduce HP peaks and the risk of cavitation [9].

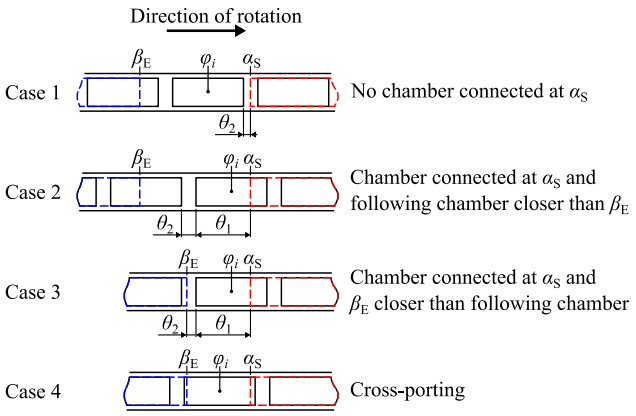

Figure 8: PP pocket position relative to effective kidney angles around commutation from LP to HP, visualised on unrolled VP.

2.2.3 Compensation Force in Contact between Valve Plate and Housing

The compensation force in the contact VP-H depends on the VP rotation angle. The different cases are shown in tab. 2 and Fig. 10. For large VP

Table 1: Constraints and variables for cases of piston pocket position relative to kidney angles around commutation.

Case	**Constraints for φ_i**	$\boldsymbol{\theta_1}$	$\boldsymbol{\theta_2}$	$\boldsymbol{\theta_3}$	$\boldsymbol{\theta_4}$
1	$\beta_{\mathrm{S}} - \gamma/2 - \delta < \varphi_i < \beta_{\mathrm{S}} - \gamma/2$	0	$\alpha_{\mathrm{S}} - (\varphi_i + \gamma/2)$	n/a	n/a
2	$\lvert\beta_{\mathrm{S}} - \varphi_i\rvert < \gamma/2$ & $\varphi_i - \gamma/2 - \delta > \alpha_{\mathrm{E}}$	$\alpha_{\mathrm{S}} - (\varphi_i - \gamma/2)$	δ	n/a	n/a
3	$\lvert\beta_{\mathrm{S}} - \varphi_i\rvert < \gamma/2$ & $\varphi_i - \gamma/2 - \delta < \alpha_{\mathrm{E}}$	$\alpha_{\mathrm{S}} - (\varphi_i - \gamma/2)$	$(\varphi_i - \gamma/2) - \beta_{\mathrm{E}}$	n/a	n/a
4	$\beta_{\mathrm{S}} - \gamma/2 < \varphi_i < \alpha_{\mathrm{E}} + \gamma/2$	0	0	n/a	n/a
5	$\alpha_{\mathrm{S}} - \gamma/2 - \delta < \varphi_i < \alpha_{\mathrm{S}} - \gamma/2$	n/a	n/a	$\varphi_i - \beta_{\mathrm{S}'} + \gamma/2$	$\beta_{\mathrm{S}} - (\varphi_i + \gamma/2)$
6	$\lvert\alpha_{\mathrm{S}} - \varphi_i\rvert < \gamma/2$ & $\varphi_i - \gamma/2 - \delta > \beta_{\mathrm{E}}$	n/a	n/a	$\varphi_i - \beta_{\mathrm{S}'} - \gamma/2 - \delta$	δ
7	$\lvert\alpha_{\mathrm{S}} - \varphi_i\rvert < \gamma/2$ & $\varphi_i - \gamma/2 - \delta < \beta_{\mathrm{E}}$	n/a	n/a	$\alpha_{\mathrm{E}} - \beta_{\mathrm{S}'}$	$(\varphi_i - \gamma/2) - \alpha_{\mathrm{E}}$
8	$\alpha_{\mathrm{S}} - \gamma/2 < \varphi_i < \beta_{\mathrm{E}} + \gamma/2$	n/a	n/a	$\alpha_{\mathrm{E}} - \beta_{\mathrm{S}'}$	0

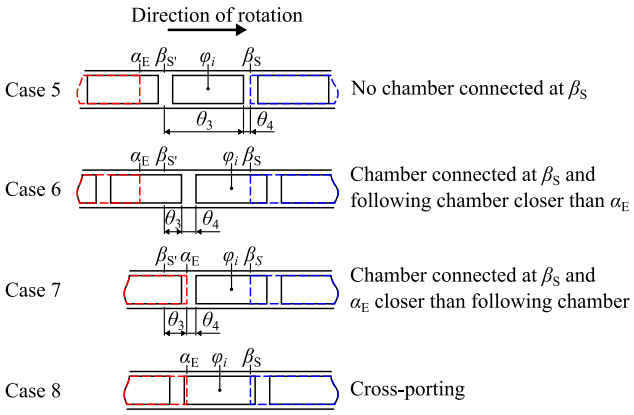

Figure 9: PP pocket position relative to effective kidney angles around commutation from HP to LP, visualised on unrolled VP.

rotation angles, the HP port in the housing partially is under the valve land as sketched in case 3 to 5, resulting in (14):

$$F_{\mathrm{HP,VP-H}} = p_{\mathrm{H}}\, A_{\mathrm{overlap}} \tag{14}$$

F_{rings} and F_{trans} are 0 when assuming perfect sealing (see sec. 2.1.3). Under

Table 2: Cases of housing ports relative to kidney for commutation from LP to HP (HP to LP is analogue).

Case	**Constraints for kidney position rel. to housing ports**	$\boldsymbol{\theta_5}$	$\boldsymbol{\theta_6}$
1	$\alpha_{\mathrm{HS}} > \alpha_{\mathrm{S}}$ & $\alpha_{\mathrm{S}} - \beta_{\mathrm{HE}} > \varphi_{\mathrm{c}}$	0	$\alpha_{\mathrm{S}} - \beta_{\mathrm{E}}$
2	$\alpha_{\mathrm{S}} - \beta_{\mathrm{HE}} < \varphi_{\mathrm{c}}$		
3	$\alpha_{\mathrm{HS}} < \alpha_{\mathrm{S}}$ & $(\alpha_{\mathrm{S}} - \alpha_{\mathrm{HS}}) < \varepsilon$	$\alpha_{\mathrm{S}} - \alpha_{\mathrm{HS}}$	$\alpha_{\mathrm{HS}} - \beta_{\mathrm{E}}$
4	$\alpha_{\mathrm{HS}} < \alpha_{\mathrm{S}}$ & $(\alpha_{\mathrm{S}} - \alpha_{\mathrm{HS}}) < \varepsilon$ & $(\alpha_{\mathrm{HS}} - \beta_{\mathrm{E}}) \geq \varphi_{\mathrm{c}}$		
5	$\alpha_{\mathrm{HS}} < \alpha_{\mathrm{S}}$ & $(\alpha_{\mathrm{HS}} - \beta_{\mathrm{E}}) < \varphi_{\mathrm{c}}$		
6	$(\alpha_{\mathrm{HS}} < \alpha_{\mathrm{E}}$ & $\alpha_{\mathrm{HE}} > \beta_{\mathrm{S}})$ or $(\alpha_{\mathrm{HS}} < \beta_{\mathrm{E}}$ & $\alpha_{\mathrm{HE}} > \alpha_{\mathrm{S}})$	n.a.	n.a.

the assumption of the presence of an oil film, F_{rings} can be calculated using (11).
Numerical calculations were carried out to calculate F_{trans} for various VP rotation angles and pressure levels for the geometry described in 3.1. This was

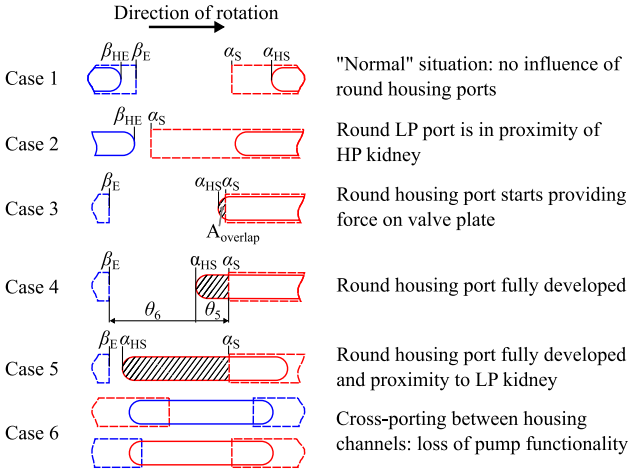

Figure 10: Position of the unrolled kidneys relative to the channels in the housing, for commutation from LP to HP (cases for HP to LP analogue). When the channels are below the valve land zone, a hydrostatic force acts on the VP.

done using the EHD simulation program described in [16], utilizing the basic functionality of modelling the geometry and solving the Reynolds equation using the finite volume method. The pressure distribution in the transition zones is extracted from the results. Fig. 11 visualises exemplary results. The results reveal that F_{trans} and its BP are scalable with the angle of the transition zone, which enables a normalisation of the results.
Attempting to generalise the results of the numerical calculations, so that forces can also be accurately calculated analytically for slightly different pump geometries (e.g., different kidney opening angles), the force of the transition area and its BP were normalised and a surrogate model was created. This surrogate model includes different equations, depending on which case in Fig. 10 is active. For cases 3 to 5 in Fig. 10, the surrogate model provides parameters for a separate calculation of the force around the round port (in the direction of θ_5) and the force in the transition area (in the direction of θ_6), see Fig. 11b.

The basis for the normalisation of the force is a fully pressurised transition area. However, (15a) considers that for large transition angles in the contact VP-H, the pressure close to the LP port is negligible, see Fig. 11. φ_{c} is the angle on which the distance on the VPs mean radius is equivalent to the

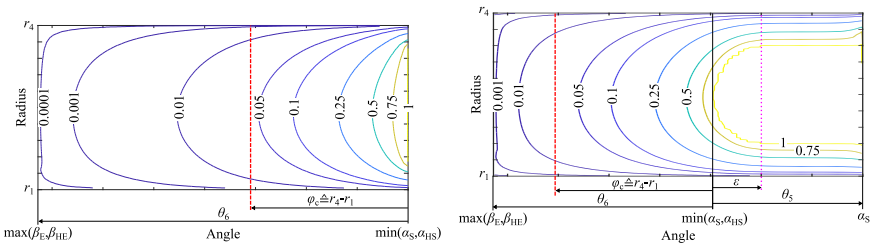

(a) Pressure distribution between two rectangular kidney ports.

(b) Distribution of normalised pressure for partially uncovered housing port. On the right hand side of the magenta colored dotted line, the pressure distribution ($p(r)$) is acc. to (10).

Figure 11: Distribution of normalised pressure in transition zone from LP to HP in VP-H contact acc. to numerical calculation, visualised on unrolled VP. The characteristic angle φ_c is the equivalent to the distance $r_4 - r_1$ on the mean radius $(r_1 + r_4)/2$. The surrogate model neglects the pressure to the left of the red dashed line.

distance between the VPs inner and outer radius. Transition areas at greater distance than φ_c are neglected.
When θ_5 is larger than the angle covered by the round end of the housing port ε, the part exceeding ε is calculated as a ring acc. to (10). Thus the angle for this area is limited to ε, see (15b). Furthermore, only the area not covered by the HP port is considered, as the area covered by the HP port is already taken into account in (14).

$$\varphi_\mathrm{p,trans} = \begin{cases} \theta_6, & \text{for } \theta_6 \leq \varphi_\mathrm{c} \\ \varphi_\mathrm{c} = (r_4 - r_1)/(\frac{r_1+r_4}{2}), & \text{for } \theta_6 > \varphi_\mathrm{c} \end{cases} \tag{15a}$$

$$\varphi_\mathrm{p,port} = \begin{cases} \theta_5, & \text{for } \theta_5 \leq \varepsilon \\ \varepsilon, & \text{for } \theta_5 > \varepsilon \end{cases} \tag{15b}$$

The surrogate model in tab. 3 provides the normalised parameters σ_F and σ_φ. Using (16), the forces and their BPs can be calculated. For the radius, no normalisation is required, as it remains almost unchanged for different φ_p. However, it needs to be considered that the housing ports of the examplary pump are not fully centred in relation to the kidney, thus the BP of the force around the port is slightly off-centre, see (16c).

$$F = \sigma_\mathrm{F}\, p_\mathrm{H}\, A \tag{16a}$$

$$\varphi_{\mathrm{F}} = \sigma_{\varphi}\, \varphi_{\mathrm{p}} \tag{16b}$$

$$r_{\mathrm{F}} = \begin{cases} \frac{r_1+r_4}{2}, & \text{for transition land} \\ \frac{r_1+r_4}{2} + 0.07\frac{r_4-r_1}{2}, & \text{for area around port} \end{cases} \tag{16c}$$

2.2.4 Influence of Valve Plate Rotation

Relative VP rotation affects the effective valve land and thus the amount of pistons loaded with HP. The pockets in the PP are directly connected to the pistons, thus the compensation force in the contact PP-VP directly reacts to an increased amount of pressurised pistons. Therefore, in the contact PP-VP, all calculations are made based on the *effective* VP angles.
In the contact VP-H, the load force is affected by relative VP rotation as it affects the amount of pressurised pistons. However, the compensation force is not affected by relative VP rotation. Thus, for the compensation force in the contact VP-H, the calculations are made based on the *total* rotation angle of each VP. In order to simplify the visualisation, the figures in sec. 3 show results for 0 deg relative VP rotation.

2.2.5 Balance Point of Uncompensated Force

The load forces are not fully compensated. The uncompensated force's magnitude can be calculated with a force balance. Its location can be calculated with a torque balance around the load force, revealing that for high compensation ratios, the compensation force can be at a significant distance from the load force (as a small compensation force requires a large lever to maintain the torque balance). The uncompensated force needs to be within the outer radius of the VP's contact surface with its contact partner in order to avoid tipping [2].

2.3 Friction Torque

The friction torque for each interface of the VP is calculated using (17). A torque needs to be provided in order to overcome this friction torque and rotate the VP.

$$T_{\mathrm{fric}} = F_{\mathrm{uncomp}}\, r_{\mathrm{fric}}\, \mu \tag{17}$$

The correct friction coefficient μ for each interface will need to be established with measurements, and even then it will not be constant over the full operating range.
Due to the different level of hydrostatic compensation, the friction coefficient

Table 3: Surrogate models for transition land force, the force from the land around the housing port and their angular location of their BPs.

Case	**Zone**	$\boldsymbol{\sigma}_{\mathrm{F}}$	$\boldsymbol{\sigma}_{\varphi}$
1	transition land	$0.243 - 1.13 \cdot 10^{-9} \cdot p/\mathrm{Pa}$	$0.267 - 5.25 \cdot 10^{-10} \cdot p/\mathrm{Pa}$
	around round port	0	n.a.
2	transition land	$0.243 - 1.13 \cdot 10^{-9} \cdot p/\mathrm{Pa} + 0.0125 \cdot (\varphi_{\mathrm{c}} - \theta_5)/\mathrm{deg}$	$0.267 - 5.25 \cdot 10^{-10} \cdot p/\mathrm{Pa} + 0.0075 \cdot (\varphi_{\mathrm{c}} - \theta_5)/\mathrm{deg}$
	around round port	0	n.a.
3	transition land	$0.243 - 1.13 \cdot 10^{-9} \cdot p/\mathrm{Pa} - 0.0109 \cdot \theta_5/\mathrm{deg}$	$0.267 - 5.25 \cdot 10^{-10} \cdot p/\mathrm{Pa} - 0.0025 \cdot \theta_5/\mathrm{deg}$
	around round port	$0.721 - 1.58 \cdot 10^{-9} \cdot p/\mathrm{Pa} - 0.0395 \cdot \theta_6/\mathrm{deg}$	$0.492 - 0.0116 \cdot \theta_6/\mathrm{deg}$
4	transition land	$0.185 - 1.13 \cdot 10^{-9} \cdot p/\mathrm{Pa}$	$0.254 - 5.25 \cdot 10^{-10} \cdot p/\mathrm{Pa}$
	around round port	$0.509 - 1.58 \cdot 10^{-9} \cdot p/\mathrm{Pa}$	0.430
5	transition land	$0.185 - 1.13 \cdot 10^{-9} \cdot p/\mathrm{Pa} + 0.0055 \cdot (\varphi_{\mathrm{c}} - \theta_5)/\mathrm{deg}$	$0.254 - 5.25 \cdot 10^{-10} \cdot p/\mathrm{Pa} - 0.0061 \cdot (\varphi_{\mathrm{c}} - \theta_5)/\mathrm{deg}$
	around round port	$0.509 - 1.58 \cdot 10^{-9} \cdot p/\mathrm{Pa}$	0.430

μ is expected to differ between the two investigated interfaces. The overall friction torque is the sum of friction torques on both interfaces. When the CB rotates at higher speed than the VP, it needs to be considered that the direction of the friction torque in the contact between VP and PP is the same as the CB rotation.
When calculating the lever/radius of the friction torque, it needs to be considered that forces can only be transmitted where contact between the parts is possible (i.e., between r_1 and r_4). Thus, the friction radius r_{fric} is approximated as the radius r_{appr} between two axial rings between r_1 and r_4 as derived in [16]. When the BP's radius r_{bp} is larger than the approximated radius, it is used instead, see (18).

$$r_{\mathrm{fric}} = \begin{cases} r_{\mathrm{appr}} = \frac{2}{3}\frac{r_4^3 - r_1^3}{r_4^2 - r_1^2}, & \text{for } r_{\mathrm{bp}} <= r_{\mathrm{appr}} \\ r_{\mathrm{bp}}, & \text{for } r_{\mathrm{appr}} < r_{\mathrm{bp}} <= r_4 \end{cases} \tag{18}$$

3 Results and discussion

3.1 Inputs

The methodology presented in sec. 2 is applied on a 35 cm^3/rev pump with 11 pistons on each side and the geometric parameters shown in tab. 4. The spring force F_{S} is 90 N and the parameter b for the pressure-dependent viscosity is set to $1.7{\cdot}10^{-8}$/Pa.

Table 4: Geometry parameters for exemplary pump.

Angles in deg	**in VP**	**in housing**	**in PP**
$\alpha_{\mathrm{S}}, \alpha_{\mathrm{HS}}, \gamma$	119.2	152.3	28.0
$\alpha_{\mathrm{E}}, \alpha_{\mathrm{HE}}, \delta$	255.2	207.7	4.7
$\beta_{\mathrm{S}}, \beta_{\mathrm{HS}}$	295.5	27.7	
$\beta_{\mathrm{E}}, \beta_{\mathrm{HE}}$	77.5	332.3	
Radii in mm	**PP-VP**	**VP-H**	**Housing ports**
r_1	26.2	27	n.a.
r_2	28.7		29
r_3	35.7		35
r_4	38.2	37	n.a.
Areas in mm^2	A_{piston}	A_{pass}	A_{kidney}
A	178.5	38.5	534.4

3.2 Compensation Ratio

Fig. 12 shows the compensation ratio for the contact PP-VP. The compensation ratio is slightly affected by the varying size of the transition area during commutation, and by the amount of pressurised pistons. VP rotation has the same effect as CB rotation on the compensation ratio.
In comparison to the analytical approaches to calculate compensation ratios which are summarised in [17], the spring force F_{S} increases the load force, and the pressure-dependent viscosity decreases the compensation force. Thus these two effects lead to a decreased result for the compensation ratio.

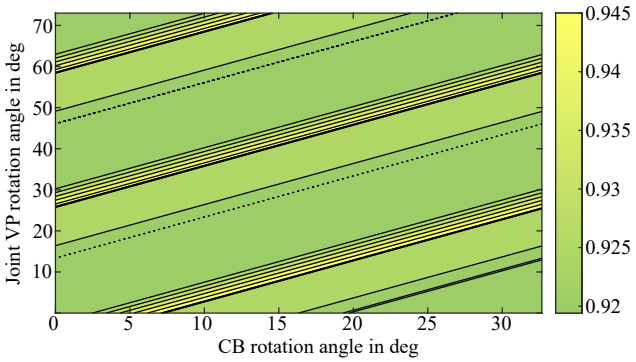

Figure 12: Compensation ratio for the contact PP-VP.

Fig. 13 shows the compensation ratio in the contact VP-H. When assuming perfect sealing (Fig. 13a), no compensation force is present until the VP reaches case 3 (see Fig. 10). With increasing VP rotation, the compensation force increases. The compensation ratio varies with the amount of pressurized pistons.
When assuming the existence of an oil film (see Fig. 13b), the compensation ratio is increased by 27 to 40%, depending on the amount of pressurised pistons. That indicates that the compensation ratio drastically increases as soon as an oil film is present between VP and housing. This case needs to be considered when targeting compensation ratios close to 1.

3.3 Location of Forces

Fig. 14 shows the location of the load force, the hydrostatic compensation force and the uncompensated force in the contact PP-VP for three different VP positions over one CB revolution. It shows that the BPs of the load force

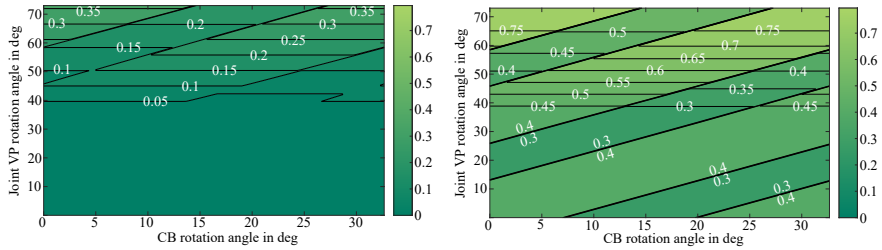

(a) Assuming perfect sealing. (b) Assuming existence of an oil film.

Figure 13: Compensation ratio in PP-H contact.

and the compensation force follow the VP rotation, and thus the uncompensated force remains inside the area of possible contact without tipping.

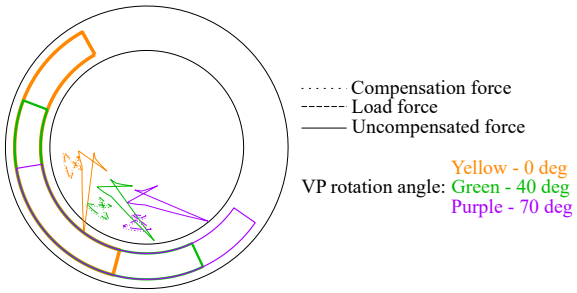

Figure 14: Location of load force, hydrostatic compensation force and uncompensated force for the contact PP-VP.

Fig. 15 shows the location of the load force, the hydrostatic compensation force and the uncompensated force in the contact VP-H for three different VP positions over one CB revolution.
Assuming perfect sealing (Fig. 15, left), there is no compensation force for small VP rotation angles. For larger VP rotation angles, the only hydrostatic compensation force is created by the pressure force from the HP port acting on the VP. The BP of this compensation force remains at a constant position over the CB rotation angle. The BP of the compensation force has a large distance to the load force. However, as the compensation force is rather small, the uncompensated force remains in proximity of the load force and within the area of possible contact for small to medium VP rotation angles. For

large VP rotation angles, the uncompensated force's BP is outside the area of possible contact, leading to VP tipping.
Assuming the existence of an oil film (Fig. 15, right), the compensation force's BP rotates with the VP. The uncompensated force's BP carries out a larger movement than the load force. When the housing port creates a pressure force on the VP, the compensation force's BP no longer fully follows the rotation of the VP. Thus, the movement of the uncompensated force's BP is increased. Even though the compensation force's BP is in closer proximity to the load force than in the scenario with perfect sealing, the BP of the uncompensated force can be even further away, as the uncompensated force's magnitude is lower and the torque balance needs to be maintained. Likewise, for large VP rotation angles, the uncompensated force's BP is outside the area of possible contact, so that tipping is expected. This reveals that VP rotation is not suitable for small displacement levels when using axial ports.

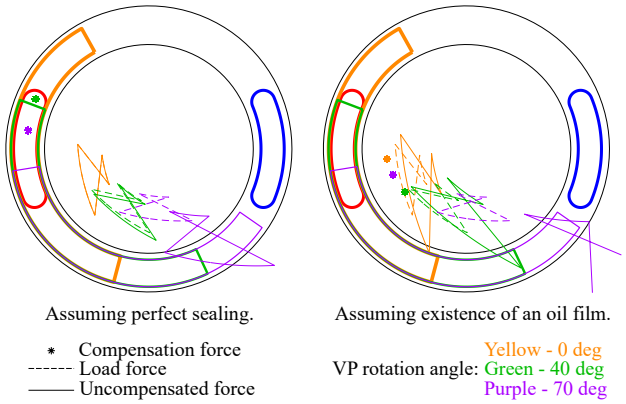

Figure 15: Location of load force, hydrostatic compensation force and uncompensated force for the contact between VP-H.

3.4 Friction Torque

Fig. 16 shows the friction torque in the contact PP-VP for an assumed friction coefficient of μ=0.06. The friction torque varies over the VP rotation angle and the CB rotation angle due to the varying amount of pressurised pistons.

Fig. 17 shows the friction torque in the contact VP-H for a friction coefficient of μ=0.12. The friction coefficient in this contact is assumed to be significantly higher than in the contact PP-VP, as the lubrication conditions

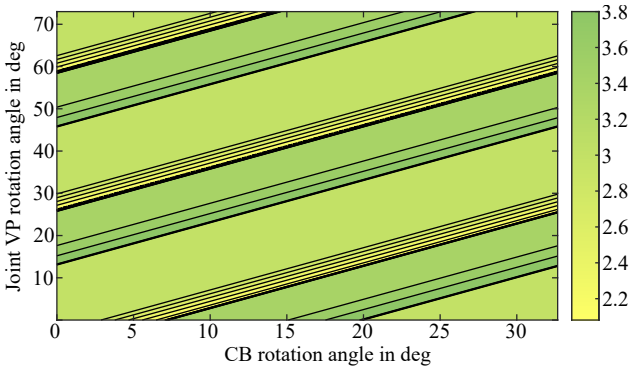

Figure 16: Friction torque in Nm at 300 bar in contact PP-VP, assuming μ=0.06.

are significantly worse (no hydrodynamic lubrication, and this contact works as seal for high compensation ratios). The friction torque strongly depends on the amount of pressurised pistons, and it decreases with increasing VP rotation angles due to increased compensation forces.
The friction torque in the contact VP-H dominates over the friction torque in the contact PP-VP.

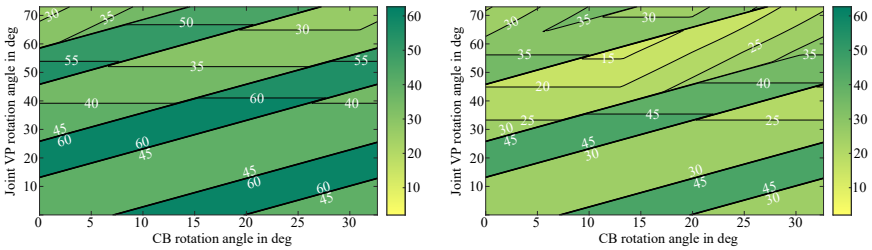

(a) Assuming perfect sealing.

(b) Assuming existence of an oil film.

Figure 17: Friction torque in Nm at 300 bar in contact VP-H, assuming μ=0.12.

3.5 Possible Valve Plate Design Improvement

In the considered exemplary pump, high friction torques occur in the contact VP-H, as compensation ratios are low. Increased compensation ratios could

decrease the friction torque. A possibility to increase the compensation ratio is shown in Fig. 18: pockets on the housing side of the VP are located adjacent to the HP kidney, providing a hydrostatic compensation force. An advantage of this pocket design is that the pockets increase the angle in which the compensation force fully follows the movement of the VP, thus keeping the BP of the unbalanced force stable over a larger VP rotation range. Furthermore, the BP of the compensation force can be moved closer to the load force. However, an (almost) full compensation of the forces in this contact is not possible, as the BP of the uncompensated force needs to remain within the outer radius of possible contact even though the compensation force does not follow the load force, and the load force varies over one revolution.

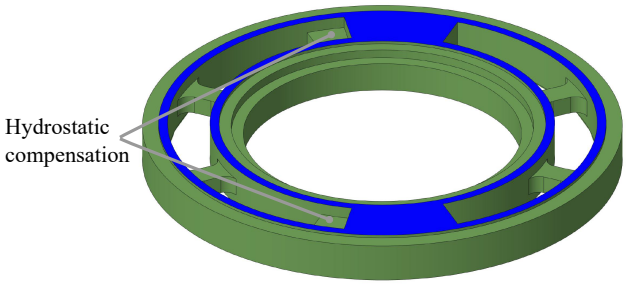

Figure 18: Partial pressure compensation with pockets on the housing side of the VP.

4 Conclusion

An analytical approach to calculate compensation ratios and friction torques for VP rotation has been presented. This has been done on the example of a double pump of floating piston type, but the approach can also be used for traditional swash plate pumps. The main share of the friction torque originates from the contact between VP and housing. Pockets for hydrostatic compensation can increase the compensation ratio and reduce this torque. However, due to the varying amount of HP pistons and the location of the compensation force does not follow the location of the load force over one revolution, a full compensation is not possible.

For large VP rotation angles, a hydrostatic force from the housing port acts on the valve plate. This force does not follow the VP rotation, leading to VP tipping. This reveals that while VP rotation provides a stable force balance

for high displacement levels, it is not suitable for small displacement levels when using axial ports.

Acknowledgment

This research was funded by the Swedish Energy Agency (Energimyndigheten, Grant Number 50181-1).

Nomenclature

Abbreviation / index	Meaning
BP	Balance point
CB	Cylinder barrel
E	End
H	Housing
HP	High-pressure
LP	Low-pressure
PP	Piston plate
S	Start
VP	Valve plate

Designation	Denotation	Unit
b	Parameter for pressure dependency of viscosity	1/Pa
h	Film height	m
p	Pressure	Pa
p_{H}	High-pressure	Pa
r, r_x	Radius	m
r_{F}	Radius of F_{trans}	m
t	Time	s
v	Velocity	m/s
A_{piston}	Piston area	m^2
A_{pass}	Area of passage in piston	m^2
A_{overlap}	Area charging the backside of the VP with HP	m^2
F_{comp}	Hydrostatic compensation force	N
F_{load}	Load force	N
F_{rings}	Compensation force from radial seal rings	N
F_{trans}	Comp. force from transition area	N
F_{HP}	Compensation force from area charged with HP	N
F_{S}	Spring force	N
T_{fric}	Friction torque	Nm
α	Angle related to HP kidney	rad
β	Angle related to LP kidney	rad
$\beta_{\mathrm{S}'}$	Angle which is $2\pi/z$ earlier than β_{S}	rad
γ	Angle covered by one pocket	rad
δ	Angle between two pockets	rad
ε	Angle covered by circular end of housing port	rad
ζ	Compensation ratio	-
η	Dynamic viscosity	Pa s
θ_x	Angular length of specific area	rad
μ	Friction coefficient	-
ρ	Oil density	$\mathrm{kg/m}^3$
σ_{p}	Factor for force in transition area / around port	-
σ_{φ}	Factor for angle of BP of force	-
φ_c	Characteristic angle	rad
φ_{F}	Angle between HP zone and BP of F_{trans}	rad
φ_i	Rotational position of piston i	rad
φ_{p}	Reference for σ_{p}	rad
φ_{E}	Angle of end of seal ring zone	rad
φ_{S}	Angle of start of seal ring zone	rad
ψ	Angle of rotation of VP	rad

References

[1] P.A.J. Achten, Z. Fu, and G.E.M. Vael. Transforming future hydraulics: a new design of a hydraulic transformer. In *The Fifth Scandinavian International Conference on Fluid Power (SICFP '97), Sweden, Linköping*, 1997.

[2] Peter Achten and Sjoerd Eggenkamp. Barrel tipping in axial piston pumps and motors. In *Proceedings of the 15:th Scandinavian International Conference on Fluid Power, June 7-9, 2017, Linköping, Sweden*, 2017.

[3] Peter A. J. Achten and Zhao Fu. Valving land phenomena of the Innas hydraulic transformer. *International Journal of Fluid Power*, 1(1):39–47, Jan 2000.

[4] Eckhard Brangs. *Über die Auslegung von Axialkolbenpumpen mit ebenem Steuerspiegel*. PhD thesis, RWTH Aachen, 1965.

[5] Junhee Cho, Xiaoping Zhang, Noah D. Manring, and Satish S. Nair. Dynamic modelling and parametric studies of an indexing valve plate pump. *International Journal of Fluid Power*, 3(3):37–48, Jan 2002.

[6] Liselott Ericson and Jonas Forssell. A novel axial piston pump/motor principle with floating pistons: Design and testing. In *BATH/ASME 2018 Symposium on Fluid Power and Motion Control*. American Society of Mechanical Engineers, Sep 2018.

[7] Liselott Ericson, Samuel Kärnell, and Martin Hochwallner. Experimental investigation of a displacement-controlled hydrostatic pump/motor by means of rotating valve plate. In *Proceedings of 15:th Scandinavian International Conference on Fluid Power, (SICFP'17), Linköping, Sweden*. Linköping University Electronic Press, Dec 2017.

[8] Thomas Grahl. Geräuschminderung an Axialkolbenpumpen durch variable Umsteuersysteme. *O+P Ölhydraulik und Pneumatik*, 33(5):437–443, 1989.

[9] Thomas Heeger and Liselott Ericson. A new degree of freedom for variable axial piston pumps with valve plate rotation. In *Proceedings of the 17:th Scandinavian International Conference on Fluid Power, SICFP21, June 1-2, 2021, Linköping, Sweden*, 2021.

[10] Jaroslav Ivantysyn and Monika Ivantysynova. *Hydrostatic pumps and motors: principles, design, performance, modelling, analysis, control, and testing*. Akademia Books International, New Delhi, 2001.

[11] Seong-Ryeol Lee, Stephan Wegner, Hubertus Murrenhoff, and Katharina Schmitz. Analytical approach to calculate the rotational angle-dependent compensation ratio of the cylinder block - valve plate contact in axial piston machines. In *16th Scandinavian International Conference on Fluid Power, SICFP'19, 2019-05-22 - 2019-05-24, Tampere, Finland*, 2019.

[12] Jan Lux and Hubertus Murrenhoff. Experimental loss analysis of displacement controlled pumps. In *10th International Fluid Power Conference, Dresden*, pages 441–452, 2016.

[13] Noah D. Manring. *Fluid Power Pumps and Motors: Analysis, Design and Control*. McGraw Hill Book CO, 2013.

[14] Hubertus Murrenhoff. *Grundlagen der Fluidtechnik, Teil 1: Hydraulik*. Shaker Verlag GmbH, Aachen, 2016. Lecture notes.

[15] Société Anonyme André Citroën. Perfectionnement aux pompes à barillet, 1959.

[16] Stephan Wegner. *Experimental and Simulative Investigation of the Cylinder Block/Valve Plate Contact in Axial Piston Machines*. PhD thesis, RWTH Aachen, 2020.

[17] Stephan Wegner, Stefan Gels, and Hubertus Murrenhoff. Vergleich analytischer Berechnungsmethoden des Entlastungsgrades im Kolbentrommel-Steuerspiegel-Kontakt in Axialkolbenmaschinen. *O+P Fluidtechnik*, pages 60–69, 11-12 2017.

[18] Jiang'ao Zhao, Yongling Fu, Jiming Ma, Jian Fu, Qun Chao, and Yan Wang. Review of cylinder block/valve plate interface in axial piston pumps: Theoretical models,

experimental investigations, and optimal design. *Chinese Journal of Aeronautics*, 34(1):111–134, 2021.

Biography

Thomas Heeger received his M.Sc. degree in mechanical engineering at RWTH Aachen University, Germany, in 2018. He is currently doing his doctoral studies in Fluid and Mechatronic Systems at Linköping University, Sweden. Research interests include pumps and their electrification.

Stephan Wegner received his Ph.D. in hydraulics from the Institute for Fluid Power Drives and Systems at RWTH Aachen University, Germany, in 2021.

Liselott Ericson received her Ph.D. in hydraulics at Linköping University (LiU), Sweden, in 2012. She currently works as a professor at Fluid and Mechatronic Systems at LiU. The areas of interest include pump and motor design, electro-hydraulic systems, modelling and simulation.